Experimental and Computational Investigation on Rotor Blades with Spanwise Blowing

Stefan Platzer [*] Jürgen Rauleder [†] Manfred Hajek [‡]

Institute of Helicopter Technology, Technical University of Munich, 80333 Munich, Germany

Joseph Milluzzo [§]

United States Naval Academy, Annapolis, MD 21402, USA

In hover, descent, and low-speed forward flight the vortices trailed from the main rotor blade tips can cause many detrimental effects associated with blade vortex interactions (e.g., high vibration and noise levels, large transient loads). Moreover, for a helicopter operating in ground effect the tip vortices can persist far downstream in the wake, which may lead to whiteout or brownout conditions. Therefore, experiments and CFD simulations were performed to investigate the ability to diffuse these tip vortices using model-scale centrifugal pumping rotor blades. In the current study, experimental and numerical investigations were combined to further increase the understanding of the modified vortex formation process, as well as to gain insight into the complex flow environment generated in the rotating channel inside the rotor blades. High-resolution particle image velocimetry was used to gain insight into the flow field generated during the initial vortex formation process. Furthermore, phase-averaged measurements were used to validate the numerical simulations. It was found that for early wake ages, spanwise blowing effectively diffused the tip vortex. The CFD simulations revealed flow details in the internal channel where experimental measurements were not possible, and it was found that the inlet geometry along with the rotor thrust level had a significant influence on the volume flow rate through the internal channel, which may ultimately affect tip vortex diffusion.

NOMENCLATURE

A	Rotor disk area, $= \pi R^2$, m^2
c	Rotor blade chord length, m
C_P	Rotor power coefficient, $= P/\rho A(\Omega R)^3$
C_T	Rotor thrust coefficient, $= T/\rho A(\Omega R)^2$
M_{farfield}	Mach number at farfield boundary
M_{tip}	Mach number at blade tip
N_b	Number of rotor blades
P	Rotor power, W
r	Radial distance from rotational axis, m
R	Rotor radius, m
Re_{tip}	Chord Reynolds number at blade tip, $= V_{\text{tip}} c\rho/\mu$
T	Rotor thrust, N
V_{tip}	Rotor tip speed, $= \Omega R$, m s^{-1}
V_{tot}	Total velocity, m s^{-1}
y^+	Dimensionless wall distance
z	Height over ground, m
ζ	Wake age of the tip vortex, $= \Omega t$, deg.
Θ_0	Blade collective pitch angle, deg.
μ	Dynamic viscosity, $kg\ m^{-1}\ s^{-1}$
$\tilde{\nu}$	Spalart–Allmaras viscosity
ρ	Air density, kg m^{-3}
σ	Rotor solidity, $= N_b c/(\pi R)$
ψ_b	Rotor blade azimuth angle, deg.
ω	Vorticity, s^{-1}
ω_{norm}	Normalized vorticity, $\omega c/(\Omega R)$
Ω	Angular velocity of the rotor, rad s^{-1}

1. INTRODUCTION

A hovering rotor wake is comprised of concentrated vortices trailed from each blade tip and turbulent wake sheets trailed from the inboard sections of the blades. After being trailed from the tip, vortices follow a helicoidal trajectory below the rotor, thereby remaining in relatively close proximity to the rotor blades for several rotor revolutions. Therefore, these dominant tip vortices can continuously interact with the rotor blades, a phenomenon known as blade

[*] Graduate Research Assistant. stefan.platzer@tum.de

[†] Assistant Professor. juergen.rauleder@tum.de

[‡] Professor and Department Head. hajek@tum.de

[§] Assistant Professor. milluzzo@usna.edu

Presented at the 42nd European Rotorcraft Forum, Lille, France, September 6–8, 2016.

vortex interaction (BVI). BVI significantly affects the local velocity fields near the blade, resulting in many adverse effects (e.g., large transient variations in the aerodynamic loads on each blade, increased vibrations, noise, etc.) (Ref. 1). Furthermore, for helicopter operations near unprepared surfaces the interaction of the tip vortices with loose mobile sediment can rapidly lead to the formation of a brownout cloud (Refs. 2–5). Many of these adverse effects could potentially be mitigated by diffusing these tip vortices. While there are many methods for achieving vortex diffusion, one potential method is the use of passive spanwise blowing (Ref. 6), which is the focus of the current work.

The vortical nature of the rotor wake has been well documented (Refs. 3, 7–20). Because the tip vortices are the dominant feature in the rotor wake a considerable amount of research has focused on their characterization (Refs. 21–32). Furthermore, as previously discussed, because of the numerous adverse effects associated with tip vortices, a significant amount of prior work has focused on altering the tip vortex structure (vortex core radius, peak swirl velocity, etc.) through the use of spanwise/chordwise blowing and blade tip modifications.

Numerous studies have investigated modifying the blade tip shape (e.g., planform, subwings, spoilers, end plates, etc.) to favorably alter the tip vortex structure (Refs. 32–41). Whereas modifications to the planform of the blade tip (taper and/or sweep) did not significantly affect the rotor performance, only modest changes to the vortex structure were observed (Refs. 32, 41). Conversely, the use of spoilers or end plates on the upper surface or trailing edge of the blade drastically diffused the tip vortices, but incurred substantial power penalties (Refs. 36, 40). A relatively effective blade tip modification was the addition of a sub-wing, however, it was susceptible to early flow separation, increased nose-up pitching moment on the rotor blade, and higher torque requirements in hover (Refs. 34, 35, 41).

Another potential method for diffusing the tip vortices is the use of active or passive flow control (Refs. 32,42–57). However, the additional power requirements, and increased nonstructural mass of actively controlled devices make them less desirable as compared to passive methods. Furthermore, passive methods are often simpler, lower cost, and have less failure modes. Therefore, tip vortex diffusion would ideally be achieved using a passive method.

Experimental and computational studies have examined the idea of using a slotted rotor blade to provide passive spanwise blowing (Refs. 6, 32, 47, 51–57). Han and Leishman (Refs. 51, 52), and Han (Ref. 53) examined the tip vortices trailed from a slotted-tip rotor blade utilizing passive spanwise blowing. The slotted-tip blade (Refs. 51–54) utilized four internal slots connecting the leading edge of the blade to its side edge (see Fig. 1) to inject small-scale vorticity and turbulence directly into the tip vortex core. The slotted-tip blade was found to produce a more diffused vortex core with peak swirl velocities nearly two-

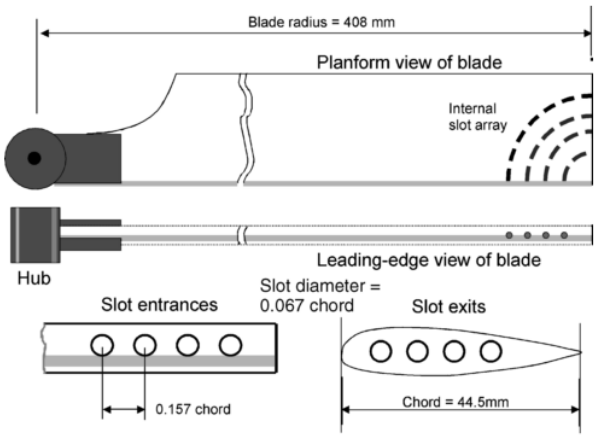

Fig. 1: Schematic of the slotted-tip blade examined by Han and Leishman (Refs. 51, 52, 54).

thirds lower than that of the baseline blade (Ref. 52). Milluzzo et al. also examined the slotted-tip blade proposed by Han and Leishman (Refs. 51, 52) on a rotor operating in ground effect as a means of modifying the tip vortices and the resulting flow at the ground (Ref. 32). They found that the slotted-tip design produced a substantially more diffused tip vortex with reduced peak swirl velocities compared to the baseline blade and little concentrated vorticity near the ground. Unfortunately, the reduction in peak swirl velocities came at the expense of a profile power penalty (Ref. 52).

The slotted-tip design (Refs. 51, 52) utilized the large dynamic pressure at the blade tip to drive air flow out the side edge of the blade (i.e., a dynamic-pressure-driven design). However, to limit profile losses it is more desirable to place the inlet slots away from the blade tip where the flow velocities and so the dynamic pressure are relatively lower. One such design places the inlet slot near the root of the blade, and uses the large centrifugal forces generated by the blade's rotation to accelerate the air radially outward. This centrifugally-driven design is also known as centrifugal pumping.

Studies were conducted by Kuerbitz and Milluzzo (Ref. 58) using performance measurements, particle image velocitmetry (PIV), and flow visualization to examine the effect pumping blades, rotor operating thrust, and exit slot orientation have on the rotor wake and tip vortices. They found that when the rotor was operated at a higher thrust condition, the pumping blade designs merely prolonged the initial formation of the tip vortices. Conversely, at the lower thrust condition the vortices were substantially diffused. Furthermore, the pumping blade designs were found to incur a power penalty, which was expected to have resulted from the exit slots at the tip increasing the profile losses, as well as Coriolis torque produced by the radial movement of air through the internal duct. However, the work by Kuerbitz and Milluzzo (Ref. 58) did not quantify the Coriolis torque. Furthermore, the details of the initial formation and roll-up of the vortices were not investigated.

Due to the difficulties associated with assessing the internal flow characteristics of rotating pipe or channel flows, only few experimental and numerical studies are available (Refs. 59, 60). Min et al. (Ref. 59) explored the ability of numerical methods to predict measured pressure distributions and mass flow rates for a centrifugally-driven flow inside a rotating duct. In this work, two predominant flow features were highlighted, namely recirculation zones and flow separation at the inlet and a mixing of the duct flow with the external flow at the outlet. Platzer et al. (Ref. 60) made a first attempt to assess the internal flow field of the centrifugal pumping rotor blade. They showed that the generic flow features observed for the rotating duct flow were also present for the centrifugal pumping blade design. Furthermore, the altered vortex formation process at the blade tip was shown in comparison to a non-pumping baseline blade including the effects of varying mass flow rates.

Pumping rotor blades were further investigated by Milluzzo et al. (Ref. 61) using performance measurements to quantify the Coriolis torque and PIV to document the initial roll-up and evolution of the tip vortices. They performed a first-order theoretical investigation of the Coriolis torque using a one-dimensional, incompressible, fully developed, steady flow analysis on the flow through the internal duct. The method yielded a simple equation that was determined to be highly dependent on the assumed conditions of the internal flow (e.g., laminar, turbulent, etc.). Furthermore, the spanwise blowing of the pumping blades initially generated a vortex core that was significantly more distorted as compared to the baseline blade, but this initial distortion was overcome by the rotation of the vortex. However, the flow through the internal duct and out of the exit slots was not examined.

To this end, the goal of the present work was to increase the understanding of the flow physics associated with centrifugal pumping rotor blades. Both experimental and numerical techniques were used to quantify the effects of passive blowing, as well as to identify areas for potential design improvements. In particular, the initial roll-up process and evolution of the tip vortices in the near-field region behind the blade were assessed and compared to a baseline blade without spanwise blowing. PIV was used to quantify the effects of blowing on the vortex formation and the results were used to assess the ability of the numerical approach to accurately simulate the rotor wake flow at early wake ages. Numerical simulations were used to reveal details of the flow physics at the inlet and inside the internal channel where measurements were not possible. Furthermore, the theoretically determined Coriolis torque was reviewed using numerical results of the internal channel flow field, and comparisons of the measured and computed power penalty associated with centrifugal pumping blades were made.

2. DESCRIPTION OF THE EXPERIMENTS

The current measurements used a two-bladed teetering rotor system with adjustable collective pitch. The rotor blades had a radius of 0.408 m (16 inches) and a constant chord of 44.5 mm (1.752 inches), which yielded a solidity of 0.0697. Each blade was comprised of a single, cambered NACA 2415 airfoil. The rotor was operated at a rotational frequency of 35 Hz (2,100 rpm), giving a tip speed of $V_{\text{tip}} = 89.72\ ms^{-1}$ (294.5 ft s^{-1}) and a nominal tip Mach number and chord Reynolds number of $M_{\text{tip}} = 0.27$ and $Re_{\text{tip}} = 282,000$, respectively. For the current measurements two different blade sets were tested, a baseline (non-pumping) blade and a pumping blade design (discussed next).

The rotor was tested in a hovering state both in and out of ground effect. For the in-ground-effect tests, the rotor was operated at a height of one rotor radius above a ground plane ($z/R = 1.0$). The ground plane was designed with a radius that was twice that of the rotor radius and with flow diverters along its circumference to limit flow recirculation. Honeycomb screens upstream of the rotor were also used to reduce the measured turbulence levels of the incoming flow to less than 1% of the average flow velocities in the rotor wake (Refs. 32, 62).

Blade Design

Flow field measurements were performed on the wakes generated by rotors with two different blade sets operating in ground effect. A rectangular (non-pumping) blade was used for a baseline. The other blade tested was a centrifugal pumping blade with a single internal duct connecting the inlet slot near the blade root to four exit slots at the blade tip; see Fig. 2. Figure 3 shows a representative image of the intake slot, which had an area of 4.011x10^{-5} m^2 (4.3174x10^{-4} ft^2). The exit slots were 3 mm in diameter and oriented such that the internal flow exited the blade along the horizontal axis (i.e., at an angle of 0°).

The inlet slot centerline was 93 mm (3.66 in) or 22.8% of the rotor radius (i.e., $r/R = 0.228$) away from the rotational axis, which yielded a flow velocity at the inlet of 20.44 m s^{-1} (67.07 ft s^{-1}). For a circle of equivalent area to the internal duct, the Reynolds number of the flow entering the duct was determined to be approximately 10,000, which was above the threshold for laminar flow (4,100).

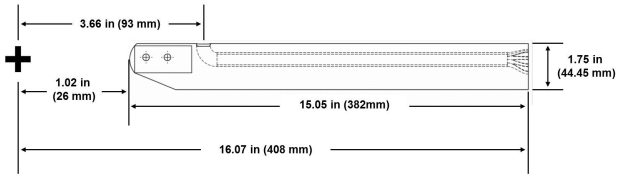

Fig. 2: Schematic of the pumping blade design with a long internal duct connecting the intake slot near the root of the blade to the exit slots at the tip.

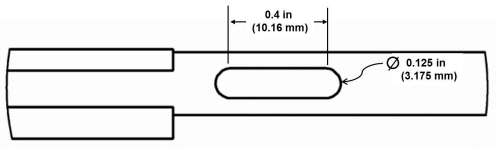

Fig. 3: Schematic of the pumping blade inlet slot near the root of the blade.

Performance Measurements

Flow field measurements were taken for the baseline and pumping blades operating in ground effect at a blade loading coefficient of $C_T/\sigma = 0.08$. Because the current performance measurements were performed on rotors operating out of ground effect, the collective pitch necessary to set the required rotor operating conditions was determined using the in-ground-effect performance measurements of Kuerbitz and Milluzzo (Ref. 58). The thrust and power coefficients were determined using the daily air density, which was calculated using ambient pressure and temperature measurements.

Flow Field Measurements

Flow field measurements were performed using particle image velocimetry (PIV), and the basic set up is shown in Fig. 4. The light sheet (approximately 2 mm in thickness) was produced by reflecting the laser beam off a high-intensity mirror and through a convex and spherical lens. The imaging axis of the camera was oriented orthogonal to the plane of the light sheet and focused on the desired region of interest (ROI). The camera and laser were digitally synchronized such that the laser pulses straddled the camera images.

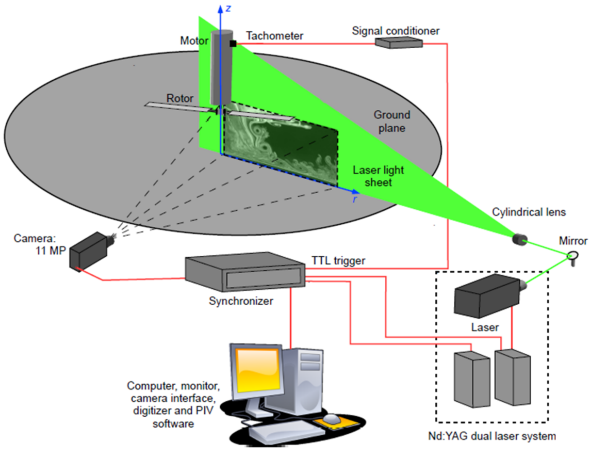

Fig. 4: Schematic showing the two-bladed rotor and the experimental setup with the laser and camera used for PIV.

Seeding Vaporized mineral oil was used to produce the seed particles for the PIV measurements. The mineral oil was vaporized in a high pressure heat exchanger, and as the vapor exited the nozzle it condensed into a fog. From a calibration, 95% of seed particles were shown to be approximately 0.22 μm in diameter, which minimized particle tracking errors (Ref. 63).

Phase-Resolved Flow Measurements The flow field measurements were obtained using a single 11 mega-pixel camera (4,008-by-2,672 pixel) and a Nd:YAG laser that was capable of emitting 532 nm light at 200 mJ/pulse when operated at a frequency less than or equal to 15 Hz. Because the rotational frequency of the rotor (35 Hz) exceeded the maximum imaging rate of the camera (1.8 Hz), the imaging system was synchronized with the rotational frequency of the rotor. Therefore, the camera was only capable of acquiring data at a sub-multiple of the rotor frequency (i.e., one image approximately every 15 rotor revolutions).

PIV Imaging The ROI for the current work where PIV measurements were taken is shown in Fig. 5 as ROI 3. It focused on a small region near the rotor blade tip to examine the initial roll-up of the tip vortex. ROI 3 had a field-of-view of 50-by-30 mm (0.12-by-0.074 R), used a laser pulse separation time of 2 μs, and 500 PIV image pairs were taken at wake age increments of 3°.

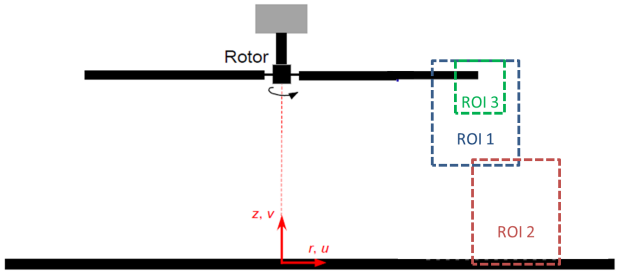

Fig. 5: Definition of the coordinate system and the regions of interest (ROIs) used for the rotor wake measurements.

For PIV cross-correlations in ROI 3, interrogation windows with dimensions of 24-by-24 pixels with a 50% overlap were used. The window size and ROI field of view provided the spatial resolution necessary to resolve the relatively steep velocity gradients found in vortex cores. An adaptive PIV method was used that automatically changed the interrogation window size and shape to optimize the local seeding density and flow gradients (Ref. 64). This adaptive PIV method provided high spatial resolution while maintaining measurement accuracy. The PIV data were processed through a local median filter that removed vectors that were more than 1.5 times the standard deviations of the median of the 3-by-3 neighboring vectors. Images containing more than 5% removed vectors were excluded from any further analysis, which comprised less than 1% of the acquired images.

3. NUMERICAL METHODOLOGY

For the present numerical study, the CFD solver TAU (Ref. 65), developed by the German Aerospace Center (DLR), was used. This finite volume solver is capable of handling unstructured as well as structured grids and has a second-order accuracy in time and space.

The viscous flow calculations were performed using the Reynolds-averaged Navier–Stokes (RANS) equations with the Spalart–Allmaras turbulence model, including a modification for negative values of the Spalart–Allmaras viscosity $\tilde{\nu}$ (SA-neg model). Multi-grid cycles were used to improve convergence. Compared to the experimental setup, the rotor hub was not modeled in the computations. Furthermore, the rotor blades were assumed to be stiff, i.e., blade flapping, bending or teetering was not modeled.

Meshing Strategy and Boundary Conditions

Fully structured grids were generated using Ansys ICEM CFD for the baseline and centrifugal pumping rotors respectively. These grids were axisymmetric to the rotational axis and consisted of approximately 66 million cells and 300 blocks. For all flow computations, a maximum dimensionless wall distance of the first cell of $y+ \approx 1$ was achieved. For the external flow, the same grid topology was used for the baseline blade (no internal channel or slots) and for the centrifugal pumping blade, including the topology at the blade tip region where the tip vortex forms (see Fig. 6). Therefore, it is assured that differences in the results were not caused by using different computational grids.

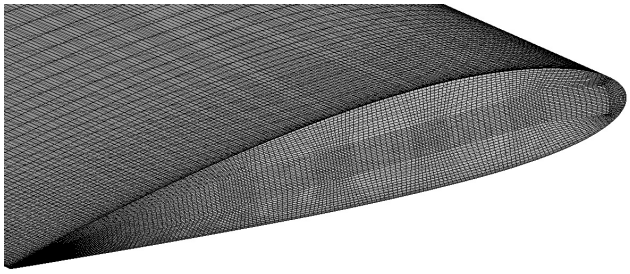

(a) Baseline Blade.

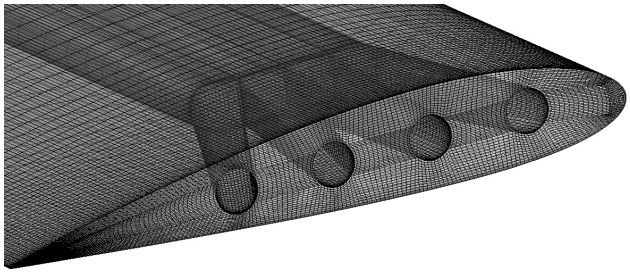

(b) Centrifugal Pumping Blade.

Fig. 6: Surface mesh at the blade tips.

The surface of the blade was resolved with 180 cells in spanwise direction and 332 cells around the blade profile (i.e., in wrap-around direction). 60 cells were placed around the circumference of the four exit slots. The development of the vortex was captured well by the finer grid around the blade. This grid design considered the fact, that capturing the vortex at its origin in the near-body grid is critical for the overall conservation of the vortices in the computational domain. The farfield boundary was placed five rotor radii away from the blade tip in radial direction and 3 rotor radii above the tip path plane (cylindrical domain with 56 c or 2.45 m radius and 37 c or 1.63 m height). To decrease numerical dissipation and dispersion and so to improve vortex preservation, a finer equidistant grid (spacing of approximately 0.061 c (2.7 mm)) was used below the blades and downstream to the ground plane. The cuboid volume of this refined grid had a side length of 22 c (0.98 m) and a height of 10 c (0.42 m); see Fig. 7.

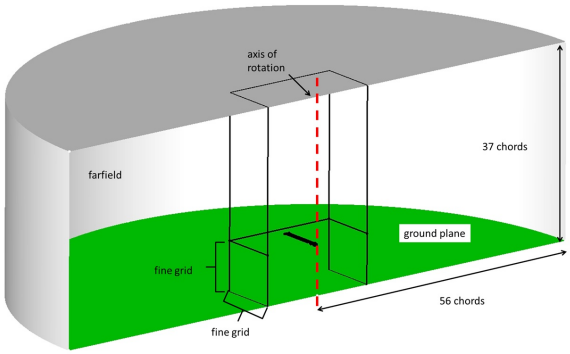

Fig. 7: Split through computational domain.

The ground plane itself was modeled as a frictionless impermeable wall, as no detailed investigation of the flow field at the ground plane was performed and the effect of a ground plane boundary layer on the flow field close to the rotor could be regarded as negligible. For the other boundaries of the computational domain a farfield boundary condition was used with a flow velocity of $M_{\text{farfield}} = 0.0$. The surfaces of the blades were modeled as fully turbulent no-slip surfaces.

By using this meshing strategy it was ensured that the vortices were preserved and convected downstream until they reached the ground plane, where they still showed similar coherence compared to what was seen in the experiments. The typical flow field for a hovering rotor in ground effect was well captured, i.e., the typical contraction and expansion of the rotor wake including the tip vortices; see Fig. 8. Because of the chosen grid generation strategy (fully structured grid including the blades without using chimera/overset grids) it was necessary to decrease the spacing right below the blades in order to be able to resolve the blade surface better. Furthermore, the grid was locally refined close to the inlet.

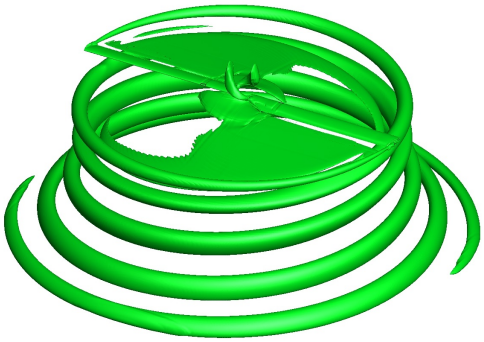

Fig. 8: Vortex visualization using the Q criterion for the pumping blade.

Convergence Criteria

For all presented computations a three-part convergence criteria was used. At first, the density residual was at least reduced by 6.5 orders of magnitude. In addition, as a second criteria at least 10,000 iterations needed to be computed to ensure that the starting vortex no longer significantly influenced the near-wake flow field and that the vortices were transported down to the ground plane. Finally, the convergence was also based on a constant rotor thrust.

4. RESULTS AND DISCUSSION

Two different test cases were evaluated, namely a zero thrust condition, $C_T/\sigma = 0.00$, and a high thrust condition, $C_T/\sigma = 0.08$. Therefore, the rotor in the numerical simulations as well as in the experiments was trimmed to meet these two conditions, which resulted in different collective pitch angle settings.

Experimental and numerical data were combined, to allow a deeper understanding of the flow physics associated with a centrifugal pumping blade design. The numerical results were validated by experimental data and the hub coordinate system was used as the reference system. As blade deformations did occur but were not measured in the experiments and they were not modeled in the simulations, deviations in the vortex positions between the experiments and the numerical simulations are partially attributed to this difference.

One focus of the study was on the vortex formation process and early wake ages ($\zeta = 3^\circ$ up to $\zeta = 12^\circ$). Moreover, numerical simulations were used to give further insight into the internal channel flow, that could not be measured experimentally at this point. For the internal flow, a special focus was put on the complex flow environment close to the inlet.

Power and Thrust Comparisons

The thrust conditions at which the experimental data were recorded were matched with a maximal deviation of 3% in the numerical simulations. For the corresponding power coefficients, C_P, larger deviations were observed (see Tables 1 and 2). At the high pitch setting a deviation of approximately 10% was computed for both blade designs. Relative differences were significantly larger for the low thrust condition.

For both thrust conditions, a nearly constant absolute difference in the power coefficients was observed between the baseline blade and the centrifugal pumping blade, i.e., the excess power required by the centrifugal pumping blade was the same in magnitude. This could be seen in the experimental as well as in the numerical results. On average, a difference of the power coefficient of $\Delta C_P = 4.85 \cdot 10^{-5}$ was measured in the experiments, whereas in the numerical simulations an averaged difference of $\Delta C_P = 5.55 \cdot 10^{-5}$ was calculated. The comparable magnitude of the excess power that was required for the centrifugal pumping blade further increased confidence in the numerical simulations and the validity of the modeled internal channel flow.

Table 1: Comparison of experimental and numerical power coefficients, C_P, at $C_T/\sigma = 0.00$.

	Baseline	Centrifugal Pumping
Experimental	$1.42 \cdot 10^{-4}$	$1.89 \cdot 10^{-4}$
Numerical	$2.51 \cdot 10^{-4}$	$3.08 \cdot 10^{-4}$

Table 2: Comparison of experimental and numerical power coefficients, C_P, at $C_T/\sigma = 0.08$.

	Baseline	Centrifugal Pumping
Experimental	$4.89 \cdot 10^{-4}$	$5.39 \cdot 10^{-4}$
Numerical	$5.35 \cdot 10^{-4}$	$5.89 \cdot 10^{-4}$

Vortex Formation Process and Early Wake Ages

In previous studies on centrifugal pumping rotor blades, early wake ages were either only considered from a numerical (Ref. 60) or from an experimental point of view (Ref. 61). Therefore, a first attempt to compare experimental and numerical results for early wake ages was made in the current work. Numerical results were validated, but also used to highlight existing shortcomings of the current CFD model. Moreover, experimental results were used to highlight the modified, transient flow field produced by the centrifugal pumping rotor blade.

In Figs. 9 and 10 total velocity contours (i.e. the in plane velocity magnitude) were compared at $\zeta = 3^\circ$ for the baseline blade and the centrifugal pumping blade, respectively. Both the experimentally determined instantaneous velocities and the numerics clearly showed the ability of the centrifugal pumping rotor blades to diffuse the tip vortex. In the measurements, a concentrated region of high rotational velocity, i.e., a concentrated vortex, was no longer visible. The same principal characteristics were found in the numerical results, with a significantly increased vortex core

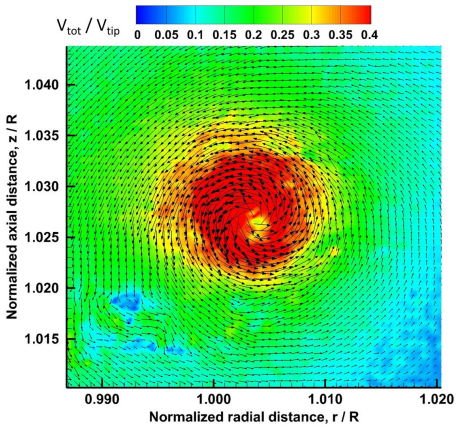

(a) Experiment (Ref. 61).

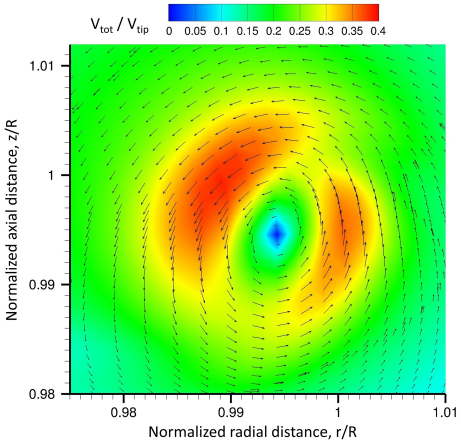

(b) Numerical Simulation.

Fig. 9: Comparison of total velocity contours normalized by the blade tip speed in ROI 3 for the baseline blade at a wake age of $\zeta = 3°$.

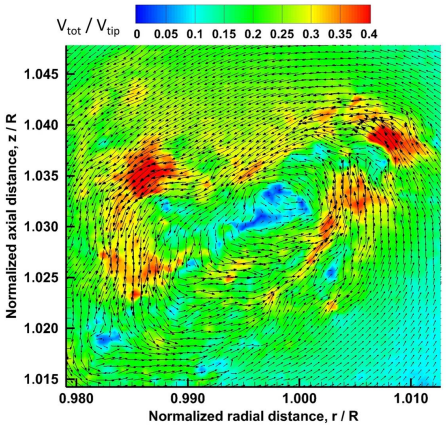

(a) Experiment (Ref. 61).

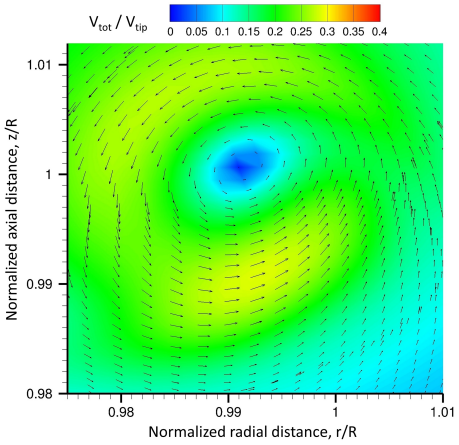

(b) Numerical Simulation.

Fig. 10: Comparison of total velocity contours normalized by the blade tip speed in ROI 3 for the centrifugal pumping blade at a wake age of $\zeta = 3°$.

size and decreased velocity magnitudes that were seen for the centrifugal pumping blade.

In the current study, the steady Reynolds-averaged Navier–Stokes equations together with a one-equation turbulence model were used. This was sufficient to predict the flow physics from a global perspective. However, the discrete intermittent regions of high flow velocities associated with the centrifugal pumping blade tip vortex could not be seen in the numerical results. These small-scale eddies, visible in Fig. 10 (a), showed significant unsteadiness along with high (velocity) gradients in the flow field. Resolving these features was beyond the capabilities of the current numerical approach as it requires finer computational grids and transient computations with sufficiently small time-step sizes. Nevertheless, the numerical approach still allowed to at least qualitatively investigate early wake ages for the centrifugal pumping rotor blade.

A comparison between numerical results and phase-averaged experimental results is given in Figs. 11 and 12. Here, vorticity contours are shown for a wake age of $\zeta = 6°$. Using phase-averaged data better resembles the characteristics of the used numerical approach, i.e., steady and Reynolds-averaged, and hence, a more valid comparison of the results is possible. In contrast to the previous comparison, the vortex core sizes correlated better, although a slight over-prediction of the vortex core growth could be observed. The vorticity levels were of comparable magnitude. Hence, it can be concluded that the numerical simulations were able to predict the phase-averaged data well, despite the under-prediction of the instantaneous values shown previously.

The comparisons discussed above showed that the used numerical approach was, at this stage, not able to accurately predict the unsteady small-scale details of the altered vortex core structure for the centrifugal pumping blade design at early wake ages. Even though a hovering rotor was considered in the present study, the roll-up process was highly transient and included numerous small-scale eddies which could not be resolved.

In previous publications, it was demonstrated that at high thrust levels the effect of blowing was most pronounced for early wake ages (Refs. 58, 60, 61). Numeri-

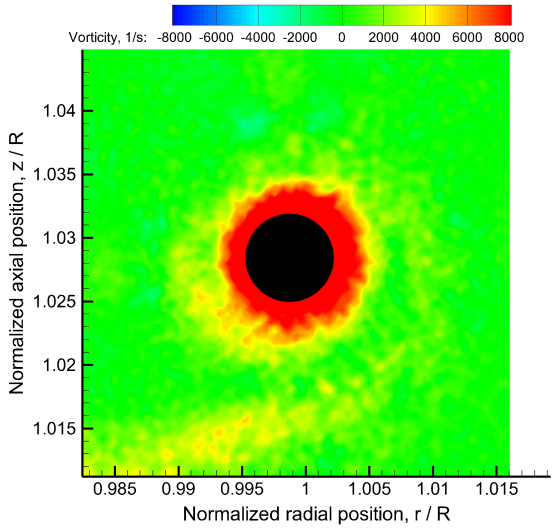

(a) Experiment (Phase averaged).

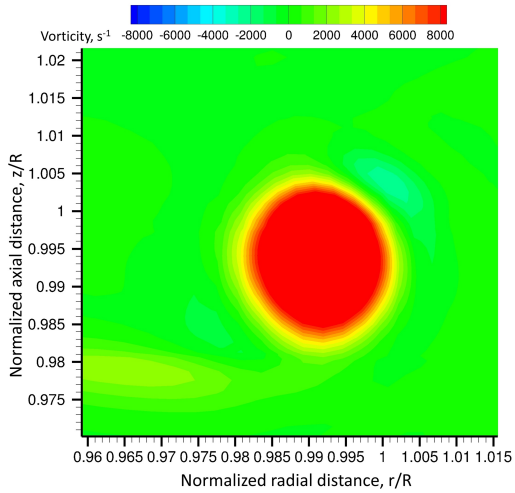

(b) Numerical Simulation.

Fig. 11: Comparison of out-of-plane vorticity in ROI 3 for the baseline blade at a wake age of $\zeta = 6°$.

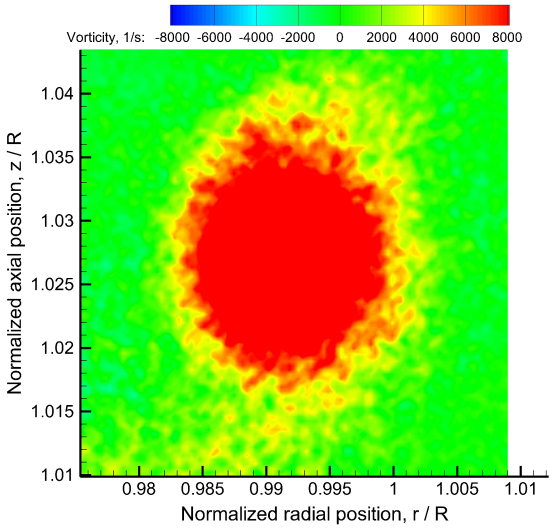

(a) Experiment (Phase averaged).

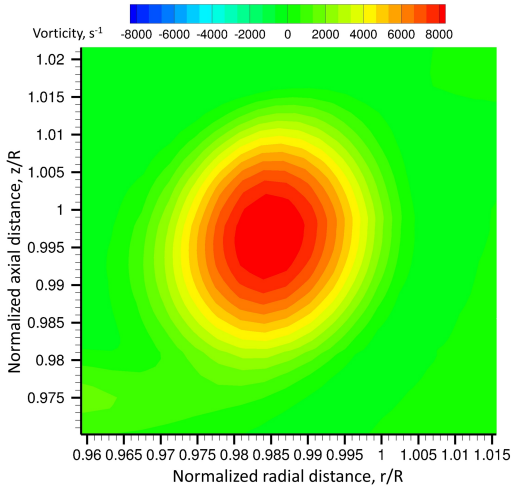

(b) Numerical Simulation.

Fig. 12: Comparison of out-of-plane vorticity in ROI 3 for the centrifugal pumping blade at a wake age of $\zeta = 6°$.

cal data (RANS calculations) was published concerning the vortex formation process at the blade and in the near field region (Ref. 60). However, thus far only little experimental data were available concerning vorticity in the flow field right behind the blade at early wake ages. Therefore, in Figs. 13 and 14 instantaneous vorticity contours for three wake ages ($\zeta = 6°$, $\zeta = 9°$, and $\zeta = 12°$) are shown for the baseline and centrifugal pumping blades. The data were normalized by

$$\omega_{\text{norm}} = \omega c/(\Omega R) \tag{1}$$

For the baseline blade, a concentrated region of high vorticity, i.e., a clearly distinguishable vortex core, could be seen. In contrast to that, and in accordance with the previous findings for the total velocity contours, a highly transient and less homogeneous flow field was visible for the centrifugal pumping blade. The passive blowing introduced small-scale eddies in the forming vortex core. In addition, the vortex size was drastically increased and no concentrated region of high vorticity could be seen any more. The positive vorticity magnitudes in the flow field were comparable for both blade designs. It is noteworthy, however, that the amount of regions with negative vorticity was significantly increased for the centrifugal pumping blade and that the eddies in these regions were also significantly stronger. These differences were less pronounced for older wake ages.

Vortex Trajectories

The overall strength, location, and size of the baseline blade's trailed vortices was in good agreement with phase-averaged experimental results for vortex wake ages ranging from $\zeta = 30°$ to $\zeta = 210°$; compare Fig. 15 and Fig. 16. For the result shown in Fig. 15, the same rotor was investigated in hover at $C_T/\sigma = 0.08$ but out of ground effect. The

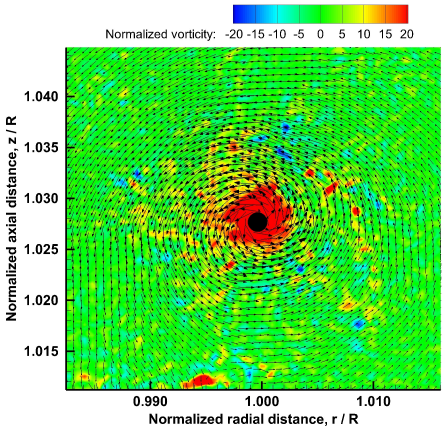

(a) $\zeta = 6^\circ$.

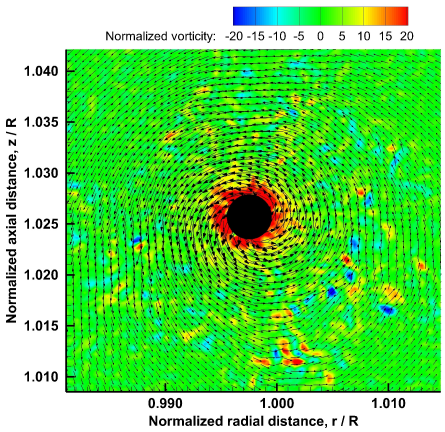

(b) $\zeta = 9^\circ$.

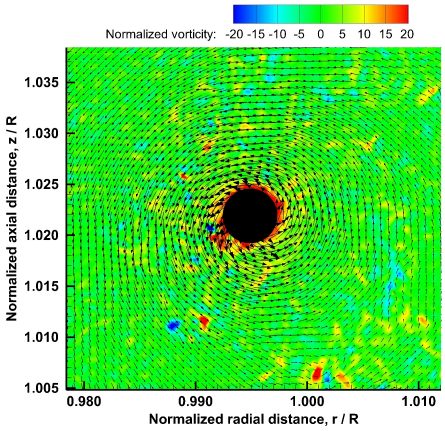

(c) $\zeta = 12^\circ$.

Fig. 13: Contours of measured normalized instantaneous vorticity in ROI 3 for the baseline blades at $C_T/\sigma = 0.08$: (a) $\zeta = 6^\circ$, (b) $\zeta = 9^\circ$, (c) $\zeta = 12^\circ$.

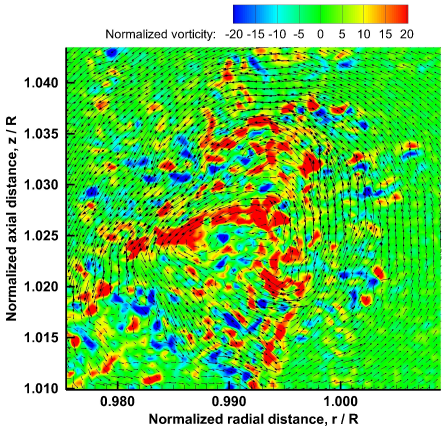

(a) $\zeta = 6^\circ$.

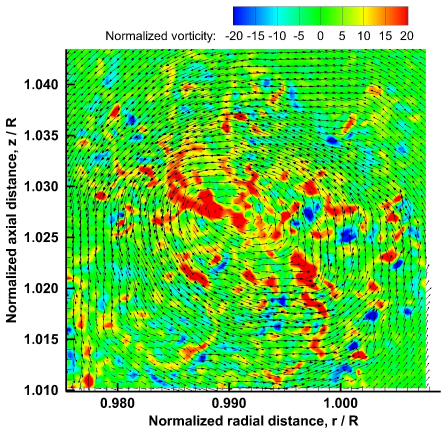

(b) $\zeta = 9^\circ$.

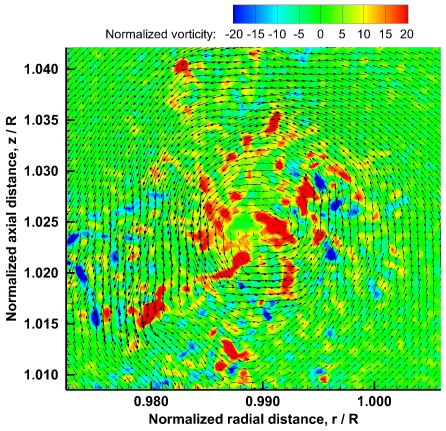

(c) $\zeta = 12^\circ$.

Fig. 14: Contours of measured normalized instantaneous vorticity in ROI 3 for the centrifugal pumping blades at $C_T/\sigma = 0.08$: (a) $\zeta = 6^\circ$, (b) $\zeta = 9^\circ$, (c) $\zeta = 12^\circ$.

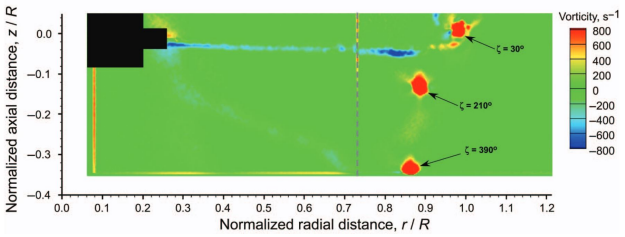

Fig. 15: Measured out-of-plane vorticity showing trajectory and strength of tip vortices for baseline blade at $C_T/\sigma = 0.08$ in hover and out off ground effect at $\psi_b = 30°$ (Ref. 66).

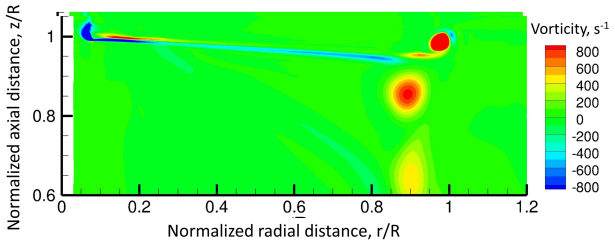

Fig. 16: Predicted out-of-plane vorticity showing trajectory and strength of tip vortices for baseline blade at $C_T/\sigma = 0.08$ and hover in ground effect at $\psi_b = 30°$.

influence of the missing ground plane on the vortex trajectory can in good approximation be neglected for early wake ages, and hence, comparing these two setups was valid. For older wake ages, $\zeta > 210°$, the vortex core size started to grow significantly in the numerical simulations. This behavior was not observed in the experiments and it was attributed to numerical dissipation. A refined grid generation strategy would be necessary in order to capture the vortex strength correctly for such old wake ages as, e.g., proposed by (Refs. 28, 55). However, these old wake ages are out of the scope of the current study.

Internal Channel Flow

The radial velocity field in the internal channel is shown in Fig. 17 for the zero thrust and the high thrust condition, respectively. It was found that the rotation of the rotor blades not only accelerated the flow in radial direction but also in chordwise direction. These coupled acceleration effects in the internal channel resulted in a nonuniform velocity profile inside the channel, i.e., the flow velocities were higher closer to the trailing edge. Therefore, greater mass flow rates were observed for the outlet ducts closer to the trailing edge compared to those closer to the leading edge of the blade.

The volume flow rate, and hence the spanwise velocity magnitude of the flow, is mostly determined by centrifugal effects. Hence, as a first order approximation, the flow rate is only defined by the rotor rotational speed. However, when comparing Figs. 17 (a) and (b), a deviation of the flow magnitudes was visible. This was also confirmed by the overall flow rates shown in Table 3. The zero thrust case

Table 3: Volume flow rates for different thrust levels.

Thrust level	Volume flow rate
$C_T/\sigma = 0.00$	0.000161 $m^3\ s^{-1}$
$C_T/\sigma = 0.08$	0.000149 $m^3\ s^{-1}$

was able to pump more fluid compared to the high thrust case. At first glance, this was unexpected, as a large region of reverse flow was visible behind the 90° corner close to the inlet for the zero thrust case, which was expected to reduce the possible volume flow rate. This region of reversed flow was also seen in (Ref. 60) for a blade loading coefficient of $C_T/\sigma = 0.07$. However, in the present study at $C_T/\sigma = 0.08$ this region was almost vanished. The only notable difference between the current study and (Ref. 60) was the higher blade pitch angle used in the present study for the higher thrust levels.

Therefore, a second mechanism must be responsible for these differences. A more detailed look at the inlet of the internal channel revealed that a second region of flow separation existed. Figure 18 shows the relative velocity between the fluid and the blade surface. As can be seen, the centrifugal pumping effect sucked fluid into the internal channel. However, for the high thrust condition a large region of reverse flow was seen as the flow separated from the lower inlet lip. This region was non-existent for the zero thrust condition. This flow separation was caused by the different collective pitch settings used for the two thrust conditions ($\Theta_0 = -2.25°$ for zero thrust and $\Theta_0 = 7.5°$ for $C_T/\sigma = 0.08$). Hence, the strong blockage effect for the high thrust condition resulted in a lower volume flow rate and lower overall flow velocities in the internal channel. This blockage, in addition to the occurring swirl flow near the lower lip, also resulted in a reduced region of flow separation behind the 90° corner; see Fig. 17 (b) and Fig. 18 (b).

It is known from previous studies on this blade design (Refs. 58, 60) that stronger tip vortices, i.e., higher thrust levels, require greater volume flow rates to efficiently diffuse the tip vortices. Therefore, the shown dependency of the volume flow rate on the set pitch angle has an adverse effects on the overall efficacy of the design to delay the vortex formation and to diffuse the tip vortex for older wake ages. However, due to the complexity of this flow and the fact that the pitch setting for the high thrust condition was slightly higher in the numerical simulation compared to the experiment, further studies have to confirm those findings. Nevertheless, improving the channel inlet design promises to be a key factor to improve the overall system performance in terms of its ability to diffuse the tip vortex.

Coriolis Torque

Although it was not possible in the current experiments to directly measure the described secondary acceleration effects, increased power requirements were measured for the centrifugal pumping blade when compared to the baseline design, which was confirmed by the numerical simu-

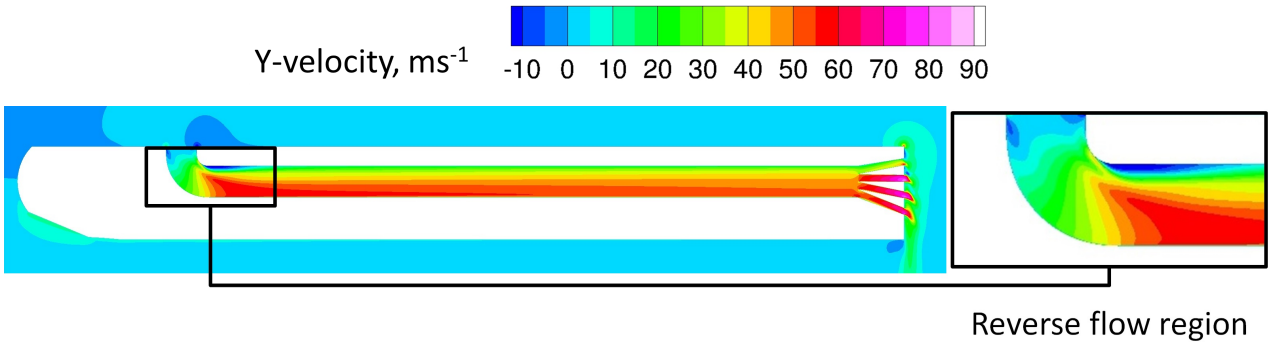

(a) $C_T/\sigma = 0.00$.

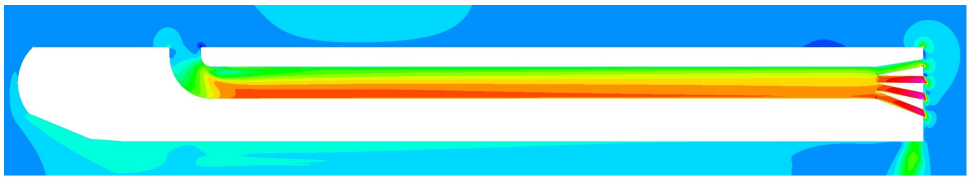

(b) $C_T/\sigma = 0.08$.

Fig. 17: Y-velocity (i.e., spanwise or radial velocity) in the internal channel for different thrust conditions.

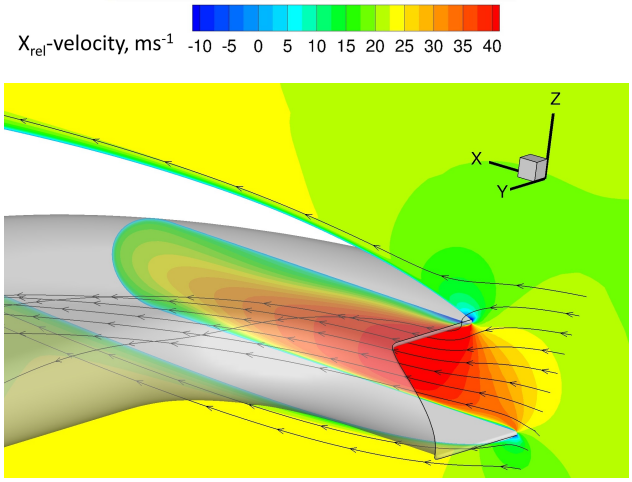

(a) $C_T/\sigma = 0.00$.

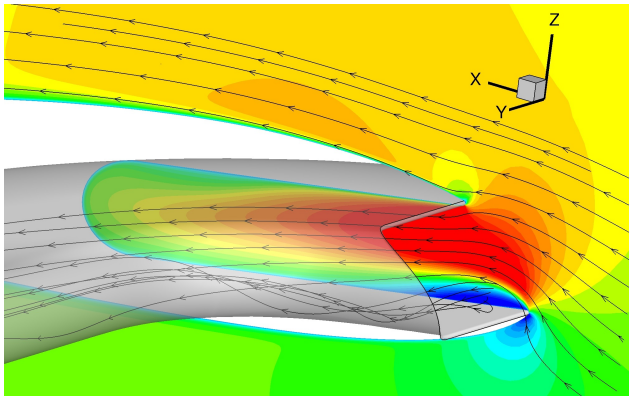

(b) $C_T/\sigma = 0.08$.

Fig. 18: Relative chordwise velocity at the inlet of the internal channel.

lations; see Tables 1 and 2. A preliminary analytical investigation based on first-order calculations revealed that Coriolis forces affecting the flow in the internal ducts are likely to be the reason for much of the additional power requirements measured for the centrifugal pumping blade (Ref. 61). When the Coriolis torque was removed, the centrifugal pumping blade had lower power requirements than a slotted blade tip (without internal channel) and it was nearly equal to the baseline blade (without blowing), particularly at high thrust conditions (Ref. 61).

For the first order (analytical) estimates (Ref. 61) the velocity distribution of a fully developed turbulent flow in a circular pipe was used, i.e., an empirical power-law velocity distribution. However, this rotationally symmetric flow field could not be confirmed by the current flow simulations; see Fig. 17. More detailed insights into the flow velocity distributions are given in Fig. 19. Radial velocity profiles were extracted from the internal channel at three different radial stations ($r/R = 0.4$, $r/R = 0.6$, and $r/R = 0.8$) for the zero thrust and the high thrust condition. These locations were chosen in regions where a fully developed flow could be assumed in the channel. In general the same global shape of the velocity profiles was found for both thrust settings. The profiles tend to reduce their asymmetric shape closer to the blade tip. This asymmetry was largest for regions closest to the reverse flow regions, i.e., for low values of r/R. The magnitude of the flow velocity was influenced by the location of reversed flow, i.e., separation at the lower inlet lip for the high thrust case reduced the overall volume flow rate and hence also the radial velocity magnitudes.

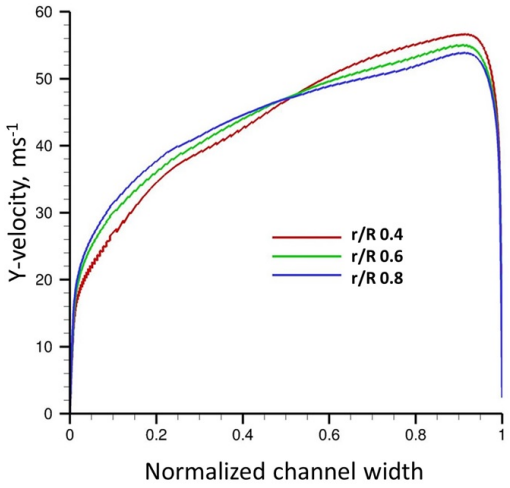

(a) $C_T/\sigma = 0.00$.

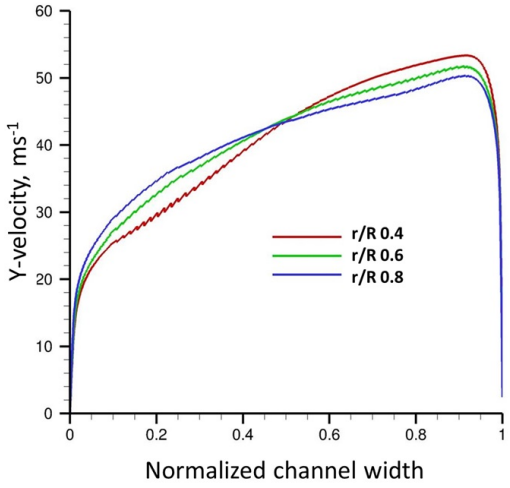

(b) $C_T/\sigma = 0.08$.

Fig. 19: Y-velocity (i.e., spanwise or radial velocity) distribution in the internal channel for three radial stations, r/R.

5. CONCLUSIONS AND OUTLOOK

Both experimental and numerical techniques were used to investigate the ability of a model-scale centrifugal pumping rotor blade to diffuse the trailed tip vortices. Specifically, the tip vortex initial roll-up and development was assessed. Furthermore, the characteristics of the flow through the internal channel were documented. Particle image velocimetry was used to quantify the initial vortex formation, as well as to provide validation for the numerical approach. The validated numerical simulations were used to provide insight into the complex flow physics in the internal channel, as well as at the inlet where measurements were not possible. The power requirements associated with centrifugal pumping rotor blades were also examined. The following specific conclusions have been drawn from this work:

1. Compared to the baseline blade, the pumping blade with passive spanwise blowing was found to produce a significantly more distorted and diffused tip vortex, which decreased the overall vorticity levels and the coherence of the vortex core. It was found that the vortex roll-up process was prolonged and that its core size was significantly increased.

2. The spanwise blowing resulted in a highly unsteady vortex formation process, which could not be picked up when using averaging techniques (i.e., phase-averaged measurements or steady RANS simulations). However, the numerical results were found to correlate well with phase-averaged measurements.

3. As was documented in previous studies, the pumping blades were observed to incur a power penalty compared to the baseline blades. The numerical simulations were able to predict the additional power requirements correctly when compared to the experimental results.

4. The numerical simulations yielded significant insights into the complex flow physics associated with the internal channel, and the resulting effects on the power requirements of the pumping blades. Specifically, the velocity profile in the channel was found to be significantly different from that found in a (standard) pipe flow, as well as those assumed in previous studies.

5. The blade pitch angle was found to have a significant effect on the formation of two reverse flow regions at the inlet of the channel, which drastically affected the volumetric flow rate through the blade's internal channel. Therefore, the Coriolis torque is also expected to be a function of the operating thrust, as well as the rotational speed, inlet and channel design.

The new results helped to improve the understanding of challenges associated with centrifugal pumping rotor blades. The combination of experimental and numerical techniques was effectively used to complement the results of the other technique and highlight possible shortcomings in the current numerical simulations. The provided insights may be used to further improve the centrifugal pumping blade design in terms of power requirements and its ability to effectively and efficiently diffuse the tip vortex at high thrust levels.

REFERENCES

[1]Feil, R., Rauleder, J., and Hajek, M., "Aeromechanics Analysis of a Coaxial Rotor System in Hover and High-Advance-Ratio Forward Flight," *34th AIAA Applied Aerodynamics Conference*, Washington, D.C., June 13–17, 2016.

[2]Rauleder, J., and Leishman, J. G., "Turbulence Modifications and Phase Couplings in Ground Effect under Simulated Brownout Conditions," *69th Annual Forum Proceedings of the American Helicopter Society*, Phoenix, AZ, May 21–23, 2013.

[3]Rauleder, J., and Leishman, J. G., "Particle–Fluid Interactions in Rotor-Generated Vortex Flows," *Experiments in Fluids*, Vol. 55, No. 3, 2014, pp. 1–15.

[4]Rauleder, J., and Leishman, J. G., "Flow Environment and Organized Turbulence Structures Near a Plane Below a Rotor," *AIAA Journal*, Vol. 52, No. 1, 2014, pp. 146–161.

[5]Rauleder, J., and Leishman, J. G., "Fluid–Particle Interaction in Vortex-Induced Dual-Phase Flows Above a Sediment Bed," *44th AIAA Fluid Dynamics Conference*, Atlanta, GA, June 16–20, 2014.

[6]Syal, M., Rauleder, J., Tritschler, J. K., and Leishman, J. G., "On the Possibilities of Brownout Mitigation Using a Slotted-Tip Rotor Blade," *29th AIAA Applied Aerodynamics Conference*, Honolulu, HI, June 27–30, 2011.

[7]Drees, J. M., and Hendal, W. P., "The Field of Flow Through a Helicopter Rotor Obtained from Wind Tunnel Smoke Tests," *Journal of Aircraft Engineering*, Vol. 23, No. 266, 1950, pp. 107–111.

[8]Gray, R. B., "An Aerodynamic Analysis of a Single Bladed Rotor in Hovering and Low Speed Forward Flight as Determined from Smoke Studies of the Vorticity Distribution in the Wake," Tech. Rep. Report No. 356, Princeton University, 1956.

[9]Landgrebe, A. J., "An Analytical Method for Predicting Rotor Wake Geometry," *Journal of the American Helicopter Society*, Vol. 14, No. 4, 1969, pp. 20–32.

[10]Landgrebe, A. J., "The Wake Geometry of a Hovering Rotor and Its Influence on Rotor Performance," *Journal of the American Helicopter Society*, Vol. 17, No. 4, 1972, pp. 2–15.

[11]Cook, C. V., "The Structure of the Rotor Blade Tip Vortex," *Paper 3, Aerodynamics of Rotary Wings, AGARD CP-111*, September 13–15, 1972.

[12]Caradonna, F. X., and Tung, C., "Experimental and Analytical Studies of a Model Helicopter Rotor in Hover," *Proceedings of the 7th European Rotorcraft Forum*, Garmisch-Partenkirchen, Germany, September 22–25, 1980.

[13]Egolf, T. A., and Landgrebe, A. J., "Helicopter Rotor Wake Geometry and its Influence in Forward Flight, Vol. 1 – Generalized Wake Geometry and Wake Effects in Rotor Airloads and Performance," Tech. Rep. CR-3726, NACA, October 1983.

[14]Lorber, P. F., Stauter, R. C., Pollack, M. J., and Landgrebe, A. J., "A Comprehensive Hover Test of the Airloads and Airflow of an Extensively Instrumented Model Helicopter Rotor," Tech. Rep. TR-D-16 (A-E), Vol. 1–5, USAAVSCOM, October 1991.

[15]McAlister, K. W., "Measurements in the Near Wake of a Hovering Rotor," *Proceedings of the 27th AIAA Fluid Dynamic Conference*, New Orleans, June 18–20, 1996.

[16]Martin, P. B., Bhagwat, M. J., and Leishman, J. G., "Strobed Laser-Sheet Visualization of a Helicopter Rotor Wake," *Journal of Flow Visualization and Image Processing*, Vol. 7, No. 1, 2000, pp. 34–54.

[17]Bhagwat, M. J., and Leishman, J. G., "Stability Analysis of Helicopter Rotor Wakes in Axial Flight," *Journal of the American Helicopter Society*, Vol. 45, No. 3, July 2000, pp. 165–178.

[18]Lee, T. E., Leishman, J. G., and Ramasamy, M., "Fluid Dynamics of Interacting Blade Tip Vortices With a Ground Plane," *Journal of the American Helicopter Society*, Vol. 55, No. 2, April 2010, pp. 1–16.

[19]Milluzzo, J., and Leishman, J. G., "Development of the Turbulent Vortex Sheet in the Wake of a Hovering Rotor," *69th Annual Forum Proceedings of the American Helicopter Society*, Phoenix, AZ, May 21–23, 2013.

[20]Milluzzo, J., and Leishman, J. G., "Quantification of the Evolution of a Vortical Sheet in the Wake of a Hovering Rotor," *44th AIAA Fluid Dynamics Conference*, Atlanta, GA, June 16–20, 2014.

[21]Tung, C., Pucci, S. L., Caradonna, F. X., and Morse, H. A., "The Structure of Trailing Vortices Generated by Model Helicopter Rotor Blades," Tech. Rep. 81316, NACA TM, 1981.

[22]Bagai, A., and Leishman, J. G., "Flow Visualization of Compressible Vortex Structures Using Density Gradient Techniques," *Experiments in Fluids*, Vol. 15, No. 6, October 1993, pp. 431–442.

[23]Leishman, J. G., Han, Y. O., and Coyne, A. J., "Measurements of the Velocity and Turbulence Structure of a Rotor Tip Vortex," *AIAA Journal*, Vol. 35, No. 3, March 1997, pp. 477–485.

[24]Mahalingam, R., and Komerath, N. M., "Measurements of the Near Wake of a Rotor in Forward Flight," *AIAA Paper 98-0692, 36th Aerospace Sciences Meeting & Exhibit*, Reno, NV, January 12–15, 1998.

[25]Leishman, J. G., Martin, P. B., and Pugliese, G., "High Resolution Trailing Vortex Measurements in the Wake of a Hovering Rotor," *Journal of the American Helicopter Society*, Vol. 48, No. 1, 2003, pp. 39–52.

[26]Ramasamy, M., and Leishman, J. G., "Interdependence of Diffusion and Straining of Helicopter Blade Tip Vortices," *Journal of Aircraft*, Vol. 41, No. 5, September 2004, pp. 1014–1024.

[27]Ramasamy, M., and Leishman, J. G., "A Generalized Model for Transitional Blade Tip Vortices," *Journal of the American Helicopter Society*, Vol. 51, No. 1, January 2006, pp. 92–103.

[28]Duraisamy, K. Ramasamy, M., Baeder, J. D., and Leishman, J. G., "High-Resolution Computational and Experimental Study of Rotary-Wing Tip Vortex Formation," *AIAA Journal*, Vol. 45, No. 11, November 2007, pp. 2593–2602.

[29]Ramasamy, M., Johnson, B., and Leishman, J. G., "Tip Vortex Measurements using Dual Plane Digital Particle Image Velocimetry," *American Helicopter Society 64th Annual Forum Proceedings*, Montréal, Canada, April 29–May 1, 2008.

[30]Johnson, B., Leishman, J. G., and Sydney, A., "Investigation of Sediment Entrainment Using Dual-Phase, High-Speed Particle Image Velocimetry," *Journal of the American Helicopter Society*, Vol. 55, No. 4, 2010, pp. 1–16.

[31]Sydney, A., and Leishman, J. G., "Time-Resolved Measurements of Rotor-Induced Particle Flows Produced by a Hovering Rotor," *Journal of the American Helicopter Society*, Vol. 59, No. 2, 2014, pp. 1–16.

[32]Milluzzo, J., Sydney, A., Rauleder, J., and Leishman, J. G., "In-Ground-Effect Aerodynamics of Rotors with Different Blade Tips," *66th Annual Forum Proceedings of the American Helicopter Society*, Phoenix, AZ, May 10–13, 2010.

[33]Landgrebe, A. J., and Bellinger, E. D., "Experimental Investigation of Model Variable-Geometry and Ogee Tip Rotors," *29th Annual Forum Proceedings of the American Helicopter Society*, Washington, DC, May 9–11, 1969.

[34]Tangler, J. L., "Experimental Investigation of the Subwing Tip and Its Vortex Structure," Tech. Rep. 3058, NASA-CR, November 1978.

[35]Berry, J. D., and Mineck, R. E., "Wind Tunnel Test of an Articulated Helicopter Rotor Model with Several Tip Shapes," Tech. Rep. 80080, NASA-TM, December 1980.

[36]Smith, D. E., and Sigl, D., "Helicopter Rotor Tip Shapes for Reduced Blade-Vortex Interaction – An Experimental Investigation," *AIAA Paper 95-0192, 33rd Aerospace Sciences Meeting and Exhibit*, Reno, NV, January 9–12, 1995.

[37]Mullins, B. R., Smith, D. E., Rath, C. B., and Thomas, S. L., "Helicopter Rotor Tip Shapes for Reduced Blade-Vortex Interaction – An Experimental Investigation II," *AIAA Paper 96-0149, 34th Aerospace Sciences Meeting and Exhibit*, Reno, NV, January 15–18, 1996.

[38]Brand, A. G., "Aerodynamic Analysis and Measurement of a Subwing Blade Tip Shape for Blade-Vortex Interaction Noise Reduction," *American Helicopter Society 53rd Annual Forum Proceedings*, Virginia Beach, VA, April 29–May 1, 1997.

[39]Russell, J., Sankar, L. N., Tung, C., and Patterson, M., "Alterations of the Tip Vortex Structure form a Hovering Rotor Using Passive Tip Devices," *Proceedings of the 53rd AHS Forum*, Virginia Beach, VA, April 29–May 1, 1997.

[40]McAlister, K. W., Tung, C., and Heineck, J. T., "Devicces that Alter the Tip Vortex of a Rotor," Tech. Rep. 2001-209625, NASA-TM, February 2001.

[41]Martin, P. B., and Leishman, J. G., "Trailing Vortex Measurements in the Wake of a Hovering Rotor with Various Tip Shapes," *American Helicopter Society 58th Annual Forum Proceedings*, Montréal, Canada, June 11–13, 2002.

[42]White, R. P. Jr., Balcerak, J. C., and Pegg, R. J., "Summary of Results Indicating the Beneficial Effects of Rotor Vortex Modification," *Proceedings of the National Symposium on Helicopter Aerodynamic Effciency*, Hartford, CT, March 6–7, 1975.

[43]White, R. P. Jr., "The Status of Rotor Noise Technology," *Journal of the American Helicopter Society*, Vol. 25, No. 1, January 1980, pp. 22–29.

[44]Dancila, D. S., and Armanios, E. A., , "Apparatus and Method for Aerodynamic Blowing Control Using Smart Materials," Tech. Rep. 5,791,601, U.S. Patent, August 11, 1998.

[45]Dancila, D. S., and Armanios, E. A., , "Apparatus and Method for Aerodynamic Blowing Control Using Smart Materials," Tech. Rep. 6,142,425, U.S. Patent, November 7, 2000.

[46]Liu, Z., Russell, J. W., Sankar, L. N., and Hassan, A. A., "A Study of Rotor Tip Vortex Structure Alteration Techniques," *Journal of Aircraft*, Vol. 38, No. 3, 2001, pp. 473–477.

[47]Dancila, D. S., *Active Rotorcraft Blade Tips for Tip Vortex Core Modifications*, Annual review of the georgia tech center of excellence for rotorcraft technology, School of Aerospace of Engineering, Georgia Institute of Technology, Atlanta, Georgia, April 8, 2002.

[48]Vasilescu, R., and Dancila, D. S., "Modeling of Piezoelectrically Modulated and Vectored Blowing for a Wing Section," *AIAA Paper 2003, The 41th AIAA, Aerospace Sciences Meeting and Exhibit*, Reno, NV, January 6–9, 2003.

[49]Vasilescu, R., and Dancila, D. S., "Electromechanical Modeling of a Piezoelectric Actuator for Modulated/V ectored Blowing," *AIAA/ASME/ASCE/AHS Structures, Structural Dynamics, and Materials Conference*, Norfolk, VA, April 7–10, 2003.

[50]Vasilescu, R., *Helicopter Blade Tip Vortex Modifications in Hover Using Piezoelectrically Moduclated Blowing*, Ph.d. dissertation, Department of Aerospace Engineering, Georgia Institute of Technology, Atlanta, GA, 2004.

[51]Han, O. Y., and Leishman, J. G., "Performance Measurements of a Rotor Blade With a Slotted Tip," *American Helicopter Society 60th Annual Forum Proceedings*, Baltimore, MD, June 2004.

[52]Han, O. Y., and Leishman, J. G., "Experimental Investigation of Tip Vortex Alleviation Using a Slotted Tip Rotor Blade," *AIAA Journal*, Vol. 42, No. 4, 2004, pp. 523–535.

[53]Han, O. Y., "Diffused Tip Vortex Structure Generated by a Slotted Tip Rotor Blade," *43rd AIAA Aerospace Science Meeting and Exhibition*, Reno, NV, January 10–13, 2005.

[54]Leishman, J. G., and Han, O. Y., "Rotor Blade System With Reduced Blade-Vortex Interaction Noise," Tech. Rep. 6,948,906 B2, U.S. Patent, September 27, 2005.

[55]Duraisamy, K., and Baeder, J. D., "Numerical Simulation of the Effects of Spanwise Blowing on Wing-tip Vortex Formation and Evolution," *Journal of Aircraft*, Vol. 43, No. 4, 2006, pp. 996–1006.

[56]Kalra, T. S., Lakshminarayan, V. K., and Baeder, J. D., "Effect of Tip Geometry on a Hovering Rotor in Ground Effect: A Computational Study," *31st AIAA Applied Aerodynamics Conference Proceedings*, San Diego, CA, June 24–27, 2013.

[57]Kalra, T. S., *CFD Modeling and Analysis of Rotor Wake in Hover Interacting with a Ground Plane*, Ph.d. dissertation, Department of Aerospace Engineering, University of Maryland, College Park, MD, 2014.

[58]Kuerbitz, D. and Milluzzo, J., "Investigation of centrifugal pumping rotor blades as a means of vortex diffusion," *Proceedings of the AHS 71st Annual Forum, Virginia Beach, Virginia, 5-7 May*, 2015.

[59]Min, B.-Y., Shannon, D., and Wake, B. E.,, "Numerical and Experimental Study of Centrifugally-Driven Flow inside a Rotating Duct for Rotorcraft Application," *Proceedings of the 72nd AHS Forum*, West Palm Beach, Florida, May 17-19, 2016.

[60]Platzer, S., Rauleder, J., and Hajek, M., "Investigation of Centrifugal Pumping Rotor Blades in Hover Using CFD," *34th AIAA Applied Aerodynamics Conference*, Washington, D.C., June 13–17, 2016.

[61]Milluzzo, J., Drayton, S., and Branson, B.,, "Performance and Flowfield Measurements of Rotors with Pumping Blades," *72nd Annual Forum Proceedings of the American Helicopter Society*, West Palm Beach, FL, May 17–19, 2016.

[62]Hance, B. T., *Effects of Body Shapes on Rotor In-Ground-Effect Aerodynamics*, M.s. thesis, Department of Aerospace Engineering, University of Maryland, College Park, MD, 2012.

[63]Leishman, J. G., "On Seed Particle Dynamics in Tip Vortex Flows," *Journal of Aircraft*, Vol. 33, No. 4, 1996, pp. 823–825.

[64]Wieneke, B., and Pfeiffer, K., "Adaptive PIV with Variable Interrogation Window Size and Shape," *The 15th International Symposium on Applications of Laser Techniques to Fluid Mechanics*, Lisbon, Portugal, July 5–8, 2010.

[65]"Description of the DLR TAU Code," *http://tau.dlr.de/code-description/*.

[66]Milluzzo, J., and Leishman, J. G., "Fluid Dynamics of Helicoidal Wake Sheets Trailed from a Hovering Rotor," *Journal of the American Helicopter Society*, Vol. 61, No. 1, 2016, pp. 11–17.